DOI:
10.1109/JSEN.2014.2328182

Document Version
Peer reviewed version

An Optical Tactile Array Probe Head for Tissue Palpation during Minimally Invasive Surgery

Hui Xie, Hongbin Liu*, Lakmal D. Seneviratne, Kaspar Althoefer

***Abstract*— This paper presents a novel tactile probe head designed for tissue palpation during minimally invasive surgery (MIS). The probe head uses fiber optics and consists of 14 tactile sensing elements at 2.5 mm spacing with a diameter of 14 mm. Each tactile element contains a micro-structure converting the tissue reaction force applied on sensing nodes into a circular image pattern through transmitting and receiving fibers. The image patterns of all the sensing elements are captured by a camera attached at the proximal end of the receiving fibers and are converted to tactile force feedback through image processing. Validation tests showed that each sensing element of the tactile probe head can measure forces from 0 to 0.5 N with a resolution of 0.05 N. The proposed sensing probe is low cost, lightweight, sterilizable, easy to be miniaturized and magnetic resonance (MR) environment compatible. Experiments were performed for testing the probe's capability of detecting the tissue abnormality through spatial distribution of tactile force feedback. The proposed tactile probe head with its capacity to accurately detect nodules embedded inside soft tissue can be an effective tool in surgical palpation during MIS.**

***Index Terms*—tissue palpation, probe head, tactile sensor, optical fiber array, MR compatible**

I. Introduction

DURING open surgery, palpation - the process where clinicians press their fingers on the patient's soft tissue organs to assess tool-tissue interaction forces- is a powerful tool in locating subsurface anatomical structures and assessing tissue properties [1]. As certain solid tumors are harder than the surrounding tissue, their presence, sizes, and locations can be obtained through tactile feedback. Manual palpation is effective in the detection of breast [2] and prostate [3] tumors, for example, and an essential means of ensuring a successful resection whilst reducing error margins. However, direct manual palpation cannot be performed through the small incisions used in minimally invasive surgery (MIS). Compared to traditional open surgery, MIS offers many advantages [4] including lower infection risks, reduced tissue trauma, and accelerated postoperative recovery. However, a major drawback of MIS is the absence of direct tissue interaction and the loss of tactile feedback [5] [6]. Surgical instruments with force sensing capability to indent, or grasp soft tissue [7] have been developed to provide surgeons performing MIS with an alternative to manual palpation. Tissue properties (e.g., size, shape, stiffness and depth) which provide the surgeon with a better understanding of internal organs during an operation [8] can be identified through mechanical soft tissue modelling and measurements of force and tissue local deformation. Numerous force and tactile sensing technologies for instrumenting the surgical devices of MIS have been developed [9] [10]. Tholey *et al*. [11] investigated current-based sensing methods in the framework of a specially designed laparoscopic grasper, which proposed a simple way to measure force in MIS. Tadano *et al*. developed a 4 degree-of-freedom pneumatic-driven forceps providing force sensing capabilities based on the measurement of air pressure. In [12], a force-sensitive probe has been created to localize lung tumors by analyzing tissue stiffness. In [13], a robotic palpation system equipped with the force/torque sensor, has been developed for examining the prostate gland. Furthermore, a rolling palpation probe, which measures the stiffness of soft tissue by rolling over it, was proposed for tissue abnormality localization in our previous work [14] [15].

The aforementioned instruments are able to measure local tissue properties but investigation of large tissue areas can be time consuming [16]. To this purpose various palpation tools using tactile array sensors have been developed to mechanically image large tissue areas. Based on resistive sensing, Schostek *et al.* [17] developed a prototype of a MIS grasper which provides both the spatial

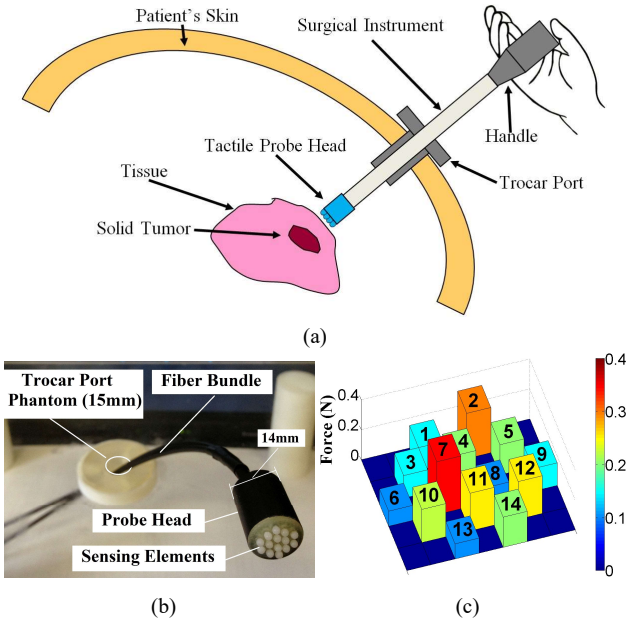

Fig. 1. (a) Application area of proposed tactile probe head, (b) Real size of the developed MRI-compatible tactile probe head, (c) Force feedback from the tactile probe head.

Manuscript received February 1, 2014. The work described in this paper has been supported by the STIFF-FLOP project grant from the European Communities Seventh Framework Programme under grant agreement 287728.

H. Xie, H. Liu, L. D. Seneviratne, K. Althoefer are with the Centre for Robotics Research, Department of Informatics, King's College London, London, WC2R 2LS, UK (*indicates corresponding author: hongbin.liu@kcl.ac.uk)

distribution and magnitudes of the applied forces. Among certain sensing principles, capacitive-based sensing is comparably efficient for measuring the applied forces and it has been widely applied in palpation. Howe *et al*. [18] have developed a capacitive tactile array remote palpation system which can measure forces with a high resolution over a range of 0 to 2 N. Rajamani's group [19] has developed a MEMS tactile sensor by using two capacitive force gauges, which are integrated under a pair of bumps with different stiffness. This sensor can quickly detect elasticity change and is capable of measuring tissue elasticity *in-vivo*. Commercial capacitive-based tactile array sensors have also been implemented in surgical palpation to localize prostate tumors [20] and to locate lung tumors [21] [22]. The main drawbacks [23] of the resistive-based and the capacitive-based tactile array sensor relate to issues of sterilization and MRI compatibility. Based on [24], the electronic components of these sensors could be damaged during the sterilization procedure, while their metallic components can introduce severe MR image distortions, a fact that prohibits their application in MRI environments. Piezoelectric-based sensors, on the other hand, do not rely on electrical power, are considered more reliable and have a wide range of applications. As an application in MIS, Dargahi *et al*. [25] developed a micro-machined tactile sensor that can be integrated in a jaw of endoscopic graspers. The drawback of piezoelectric materials is that they are only sensitive to time-varying forces and changes in temperature [26].

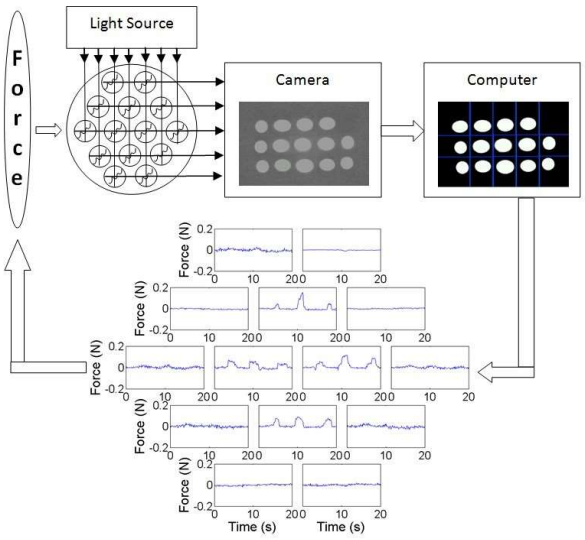

Fig. 2. Schematic design of proposed tactile sensor using camera.

The fiber optic based tactile sensing method is an effective way to equip medical tools with the force measurement capability within a high intensity electromagnetic field. An optical fiber sensor uses four main sensing mechanisms, namely, wavelength, phase, polarization and intensity modulation [27]. All of these mechanisms consist of a light source, transduction and detection parts. In this paper we use the light intensity modulation method [28] [29] as it is versatile, inexpensive, temperature insensitive and easy to fabricate. Most of the existing intensity modulation fiber optic force sensors [30] [31] use individual phototransistors or photodiodes to convert light intensity into voltage signals, which are converted into force information through calibrations.

A different method of light intensity modulation has been developed by this team [32]. Instead of using individual photo-electronic for each sensing element, only one low cost CMOS USB camera is employed to capture and detect the light intensity changes of all sensing elements. The signals are then processed in Matlab/Simulink and converted to a tactile map. Previous research [33] [34] [35] on camera-based tactile sensors focused on analyzing image pattern from the small-sized camera integrated at the tip of tactile sensors. In our case, the light signals are transmitted by optical fibers, thus there is no need for the detection camera to be placed near the tip. This allows the tactile sensor to be further miniaturized and to work in an MR environment as the detection camera can be placed out of MR range.

In this paper, an optical tactile array probe head for tissue palpation during minimally invasive surgery is presented, (Fig. 1). The sensing system proposed in this paper is low cost, small in size, lightweight, free from electromagnetic interference, water and corrosion resistant and capable to operate in harsh environments. The original design of the tactile sensor proposed in our previous work [32] has been further modified and miniaturized for application in surgical palpation during MIS. In addition, the proposed new sensor has increased sensitivity and reduced crosstalk. This optical fiber-based sensing system has potential for the medical applications because it can be sterilized and is MRI compatible. The developed probe head can be integrated with various types of medical tools during operations while its low manufacturing cost allows it to be single-use only. The probe head presented in this paper has a diameter of 14 mm and can be used through a 15 mm trocar port during MIS [36]. Due to its design simplicity, the proposed tactile probe-head can be readily miniaturized further to fit in smaller trocar ports or even provide tactile force feedback from a catheter-tip (4-8 mm). The proposed probe head is based on our previous work [37] and has been further miniaturized to fit a 15 mm trocar port, and has increased sensing elements, thus providing a more detailed tactile information. Also the relationship between the optimal light response and the displacement change has been investigated, together with the dynamic response of the tactile sensor. Experiments were carried out on silicone phantom and lamb kidney with simulated tumors in order to produce stiffness map. The results demonstrate that the probe head was able to produce a high resolution stiffness map which can clearly indicate tumor locations.

II. METHODOLOGY

The schematic design of the presented sensor to explain the sensing methodology is shown in Fig. 2. The light source transmits the light to the sensing area, which is 14 mm in diameter with 14 sensing elements. When force is applied to a sensing element, the displacement change of the flexible material varies the light intensity observed by the receiving fiber. The image of the light

intensity distribution is captured by the camera attached at the end of the receiving fiber, and is converted to spatial contact forces through image processing.

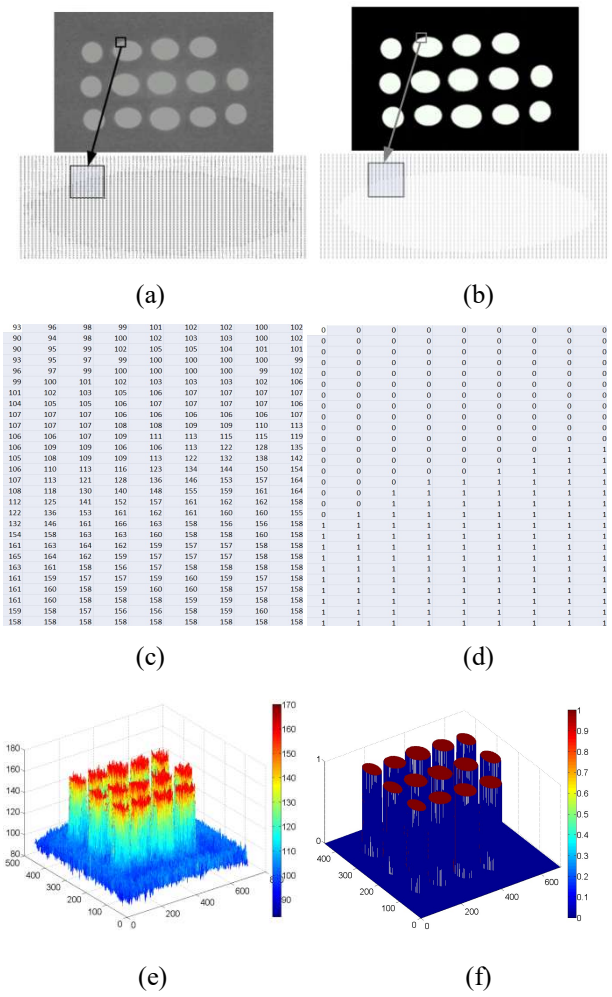

Fig. 3. Sequence of Image Processing before and after thresholding: (a) gray scale images captured by camera, (b) binary image after thresholding, (c) gray value of individual pixel, (d) binary value of individual pixel, (e) intensity map of gray scale picture, (f) intensity map after thresholding.

A. *Processing of light intensity image*

In order to extract useful information while at the same time removing the background noise of the light intensity image, we converted the gray scale image into binary image, Fig. 3. A variety of thresholding methods, such as the point-dependent and the region-dependent method [38], have been proposed in the past where the threshold value is determined either by the gray level of each individual pixel or the local gray level neighbouring each pixel. A global thresholding method [39] is giving one threshold value to the entire picture, while a local one [40] provides different values to sub-images. To deal with the high contrast of background and object in the light intensity image, we have used here a thresholding method in which the valley of the histogram is defined as the threshold value [41]. Compare to previously described thresholding methods, this is a more straightforward method and has with less computational complexity. We define $f(x, y)$ as the gray value of the pixel coordinated at (x, y) in the image with a size of x_{max} by y_{max}.

$$f(x, y) \in \{0,1,2 \ldots,255\}, \quad (1)$$

where $1 \leq x \leq x_{max}$, $1 \leq y \leq y_{max}$, 0 stands for the darkest pixel and 255 for the brightest pixel. Each pixel value is converted from gray scale (0-255) to either 0 or 1 utilizing the following equation:

$$f_T(x, y) = \begin{cases} 0, if\ f(x, y) < I_{threshold} \\ 1, if\ f(x, y) > I_{threshold} \end{cases}, \quad (2)$$

where $I_{threshold}$ is the threshold value to eliminate ineffective pixels from the background, $f_T(x, y)$ is the value of pixel at (x, y) after thresholding. The real-time image is divided into 14 sections, each representing one single sensing element. The activate pixel number N of each section is given by:

$$N = \sum f_T(x, y), \quad (3)$$

where N is the total value of the pixels in each sensing area, the size of the section is x_{max} by y_{max}. The relation between force f and pixel value N is further investigated and demonstrated in sections below.

B. *Probe head Design*

The proposed probe head design consists of two plastic optical fiber bundles (SH1016, Mitsubishi Rayon Co., Ltd., Tokyo). Each bundle contains 16 individual optical fibers with a core diameter of 0.231mm to 0.279mm. The core refractive index of each fiber is 1.49 and the numerical aperture is 0.50. One fiber bundle is used for transmitting light from the light source while the other for receiving light to the camera. The individual fibers are fixed on the supporting base (Fig. 4). The developed sensor prototype, shown in Fig. 5, was designed in Solidworks (Solidworks Corp., MA) and printed by a rapid prototype machine (Projet HD 3000 Plus, 3D-Systems, SC). In this paper, the sensor is fabricated using ABS (acrylonitrile butadiene styrene) material which is light-weight, free from most of the chemically corrosion and MRI compatible.

Latex rubber is used as the flexible structure between the supporting material and sensing tip. The higher the value of applied force is, the bigger the deformation of the rubber. The supporting structure is designed with 14 separate grids to isolate the deforming area of each individual sensing element from the adjacent elements, preventing crosstalk. There are 14 cylindrical sensing units with a ball shape tip. Below each unit, a concave aluminium surface is attached to reflect light from the transmitting fiber to the receiving fiber, enabling more effective light transmission between fibers. As the sensor detects z-axis force information only, a top layer is designed to constrain the x and y-axis movements of the sensing units.

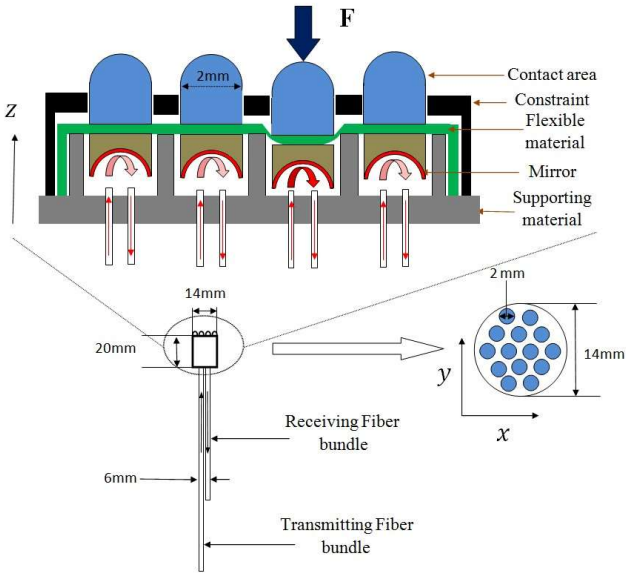

Fig. 4. Schematic drawing of the probe head design and assemblies.

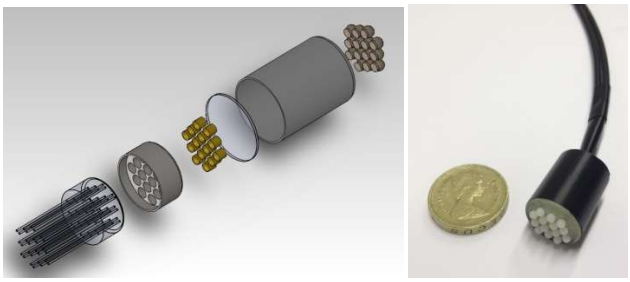

Fig. 5. The prototype of the tactile probe head.

Four different patterns of the reflective surface have been investigated as shown in Fig. 6. One reflective surface is flat while the other three have ellipsoidal concave shape with same minor radius of 1 mm but different major radius r (0.5 mm, 1 mm and 2 mm). A pair of transmitting and receiving fibers (core diameter 0.25mm, refractive index 1.49 and numerical aperture 0.50) is placed in parallel with a distance of 1mm between them. A fiber optic illuminator (Fiber-Lite 3100, Dolan-Jenner Industries, MA) is used for providing a stable light source at a wavelength of 560 nm; a low-cost CMOS HD camera (Microsoft LifeCam Studio, Microsoft, WA) is used as the receiver and controlled by MatLab (Mathworks Inc., MA). All parameters of the camera (e.g. autofocus, zoom, white balance and aperture) were kept constant during the test. The aluminium tape (Maplin Electronics Ltd, UK) is used as reflective surface attached to ABS support with different inner structure.

To evaluate a different reflective surface, the light intensity images are recorded while the distance between the reflector and fiber is changing with increments of 0.1mm from 0 to 2.5mm. For each reflective surface, tests are repeated 10 times. The results are shown in Fig. 7. It was found that the flat reflector introduced a high level of error and that no light signal could be detected after 1.5mm. This may have been caused by the scattering of the light. On the other hand with a concave shaped reflector, error was relatively low and the light signal started to decrease significantly at 1.5 mm and up to 2-2.5 mm. The proposed sensor requires a relatively linear response within a displacement range of at least 0.5 mm, allowing the flexible structure to deform so that it can detect forces. From the test results, the concave reflector with medium radius (r=1 mm) is chosen, utilizing its response range of 2-2.5 mm.

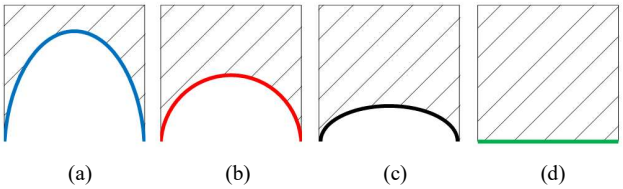

Fig. 6. Different patterns of reflection shape for testing the relationship between displacement and light intensity change: (a) reflector with small major radius ($r = 0.5\,mm$), (b) reflector with medium radius ($r = 1\,mm$), (c) reflector with big radius ($r = 2\,mm$), (d) flat reflective surface ($r = \infty$). r is the major radius of the ellipse.

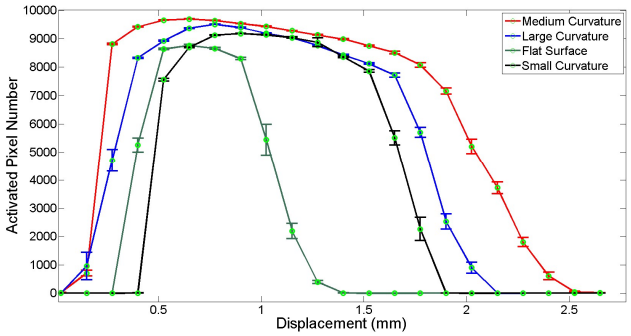

Fig. 7. Relationship between light intensity (activated pixel numbers) and displacement change.

III. Experimental Results

The experiment set-up for tactile probe head testing is shown in Fig. 8. The same light source (Fiber-Lite 3100 Dolan-Jenner Industries, MA) is used during the test. A USB camera with high-definition is used to transfer the image of light intensity to the computer for further analysis. An ATI Nano 17 Force/Torque sensor together with a data acquisition card (NI USB-6341, National Instruments, TX) is used for calibrating the proposed tactile probe head.

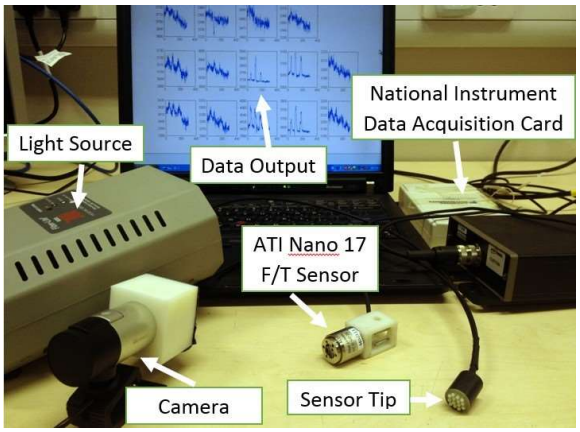

Fig. 8. Equipment Set-up.

A. Calibration

Before using the tactile probe for palpation, calibration is essential. To conduct calibration, the tactile sensor was mounted on a rigid static support, as shown in Fig. 9, and the 14 sensing elements were loaded individually using the

ATI Nano 17 Force/Torque sensor, at increments of 0.05 N from 0 N to 0.4 N. The real-time image data is recorded by the camera and converted to distributed force information through the image processing procedure elaborated in Section II.A. Fig. 10 shows the relations between activated pixels and applied forces of sensing element 1 for both linear and quadratic fitting. The quadratic and linear relationship between the sensor output, which is the pixel number, and applied force are represented by

$$N = \alpha f^2 + \beta f + \gamma, \quad (5)$$

$$N = \delta f + \quad , \quad (6)$$

where N is the output of the sensor, f is the force on individual sensing element and α, β, γ, δ, ε are the calibration coefficients, which are listed in Table I and Table II together with respective R-squared values.

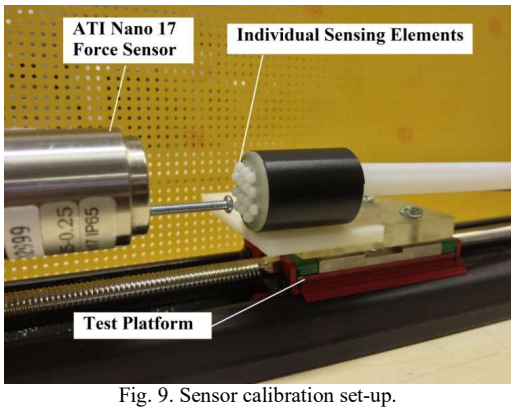

Fig. 9. Sensor calibration set-up.

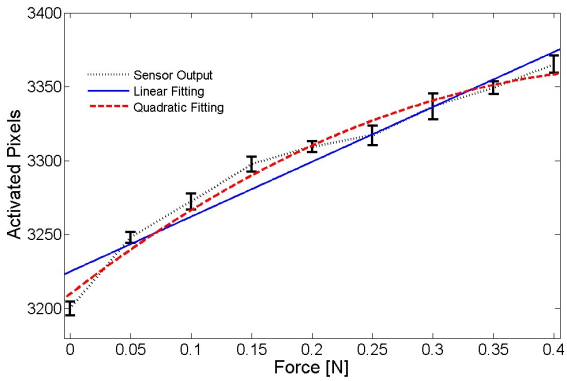

Fig. 10. Measured output responses of sensing element 1 to the normal force applied.

TABLE I. COEFFICIENT OF LINEAR FITTING CURVE

Sensor Number	Coefficients		
	δ	ε	R_o^2
1	18.559	3206.7	0.9435
2	14.995	3548.8	0.8814
3	8.4941	3022.7	0.688
4	19.297	3721.5	0.9735
5	9.1086	3246.1	0.963
6	8.2409	3349.8	0.7241
7	37.468	3423.1	0.9797
8	24.012	3662.2	0.8967
9	55.899	3443.9	0.924
10	34.74	3065.4	0.7354
11	47.833	3202.1	0.9246
12	46.17	3544.8	0.8083
13	48.63	3114.2	0.9386
14	13.612	3088.4	0.9301

TABLE II. COEFFICIENT OF QUADRATIC FITTING CURVE

Sensor Number	Coefficients			
	α	β	γ	R^2
1	-1.6259	34.817	3176.9	0.9807
2	-1.3906	28.901	3523.3	0.9203
3	-1.997	28.464	2986.1	0.8832
4	0.1055	18.242	3723.4	0.9737
5	-0.399	13.099	3238.8	0.9724
6	-1.8894	27.135	3315.2	0.9195
7	-1.0061	47.529	3404.6	0.9833
8	-2.84	52.412	3610.1	0.961
9	-2.3967	79.866	3400	0.9328
10	7.6529	41.789	3205.7	0.9186
11	-2.7513	75.346	3151.6	0.9403
12	-8.2542	128.71	3393.5	0.9409
13	-0.5315	53.945	3104.4	0.9392
14	0.9179	4.4338	3105.3	0.9518

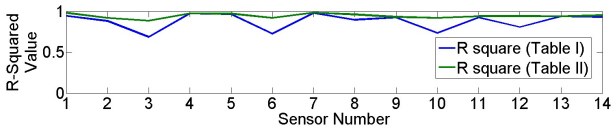

Fig. 11. Comparison of R-square value between Table I and Table II.

By comparing the R-squared values between Table I and II in Fig. 11, it can be concluded that quadratic fitting for each sensing element have higher R-squared values than linear fitting. In Table II it can be seen that the sensor has a reasonable linearity between sensor output and applied force with most of the R-squared values close to 1. Each sensing element has been tested 10 times and the standard deviations are seen by the error bars corresponding to every increment.

B. Dynamic Response and Shape detection

After calibration, the dynamic response of the proposed sensor was investigated. Same as the static calibration procedure, the sensor was placed onto the linear actuator controlled manually and was in contact with the Force/Torque Nano17 sensor. The responses of one single sensing element and the Nano17 sensor are illustrated in Fig. 12. The test results demonstrated that the proposed sensor is capable of providing accurate measurements with a frequency up to 10 Hz. Also it can be seen that the crosstalk between sensing elements is relatively small due to the particular mechanical design of the sensor. The root mean square error (RMSE) is 0.0184 N (less than 5% of total amplitude range). The accuracy of all sensing elements is presented in Fig. 13, with the minimum value of 90%. The error is mostly due to the hysteresis effect of the rubber and the light signal loss by fiber bending and connection [42], which will be considered in the future research related to both hardware design and software optimization.

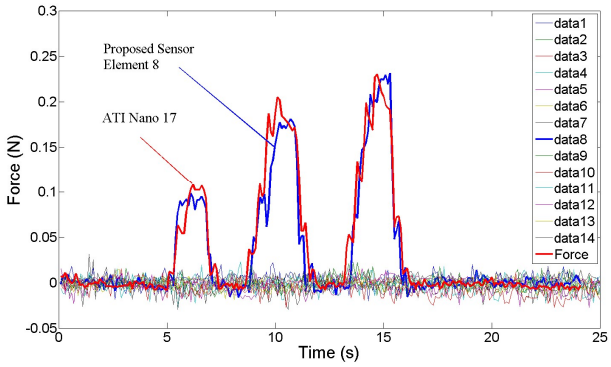

Fig. 12. Proposed sensor responses under inputs with variable amplitudes from commercial force sensor.

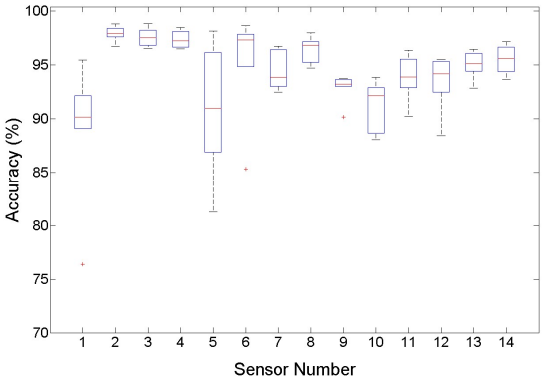

Fig. 13. The accuracy of each sensing elements on the proposed tactile array probe head.

After evaluating an individual sensing element of the probe head, shape detection tests are conducted using a cylinder shape plastic object with a flat round tip fixed on the platform. Then the probe head was placed lowered on to the object until a firm contact with the object occurs, as shown in Fig. 14. The test was repeated three times. To intuitively view the test results, the responses of all sensing elements were displayed according to their placement shape on the probe head, as shown in Fig. 15. From the results, it can be seen that the four sensing elements which were in contact with the object had a force feedback higher than 0.05 N, while the other 10 sensing elements' responses were within the noise range of ± 0.03 N. The uneven force distribution on four contacting sensing elements may be caused by a different contact angle between sensor and object, the stiffness variation through the rubber and the hysteresis effect. However, the detecting forces are all within 0.05-0.15 N which demonstrates the usefulness of shape detection.

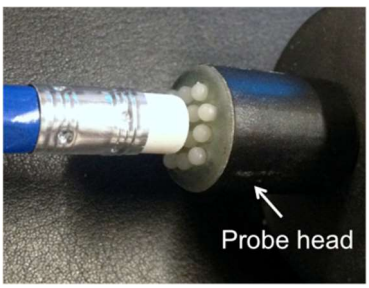

Fig. 14. Shape detection test; a cylindrical object with flat round tip is in contact with four central sensing elements on the probe head.

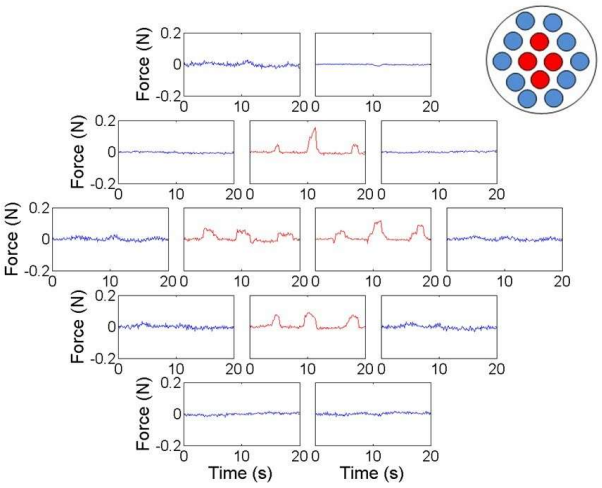

Fig. 15. Displacements of the output of each sensing element on the probe head.

C. *Experimental Results of Tissue Palpation*

The tissue palpation experiment was conducted by mounting the tactile probe head on a robot arm (Mitsubishi RV-6SL). During tests, the probe head palpated on a planar surface silicone phantom tissue made of RTV6166 (General Electric Corp., CT) (ratio: 30/70, density: 1100 kg/m^3, sound speed: 1050 m/s, attenuation: 3.45Np/m/MHz, Young's modulus: 15.3 kPa [43] [44]), shown in Fig. 16. The silicone phantom had two spherical nodules (Staedtler Mars plastic 526-50, Staedtler Mars GmbH, Nurnberg, Germany) with the hardness of 47-50 Shore A, which were embedded at a depth of 6mm, as shown in Fig. 17 (a). The tactile probe head was maneuvered to conduct a series of indentations on the phantom tissue surface to cover the area A where the 2 nodules were located, Fig.16. The indentation depth was 2mm; the lateral distance between two adjacent indentations was 14 mm which is the size of the probe head. Considering the light loss due to fiber bending, the tactile sensing units of the probe head was recalibrated after being mounted on the robot arm. The palpation tests were repeated ten times, during which the bend radius was approximately constant. By fusing the palpating locations of the probe head and the locally measured force distributions by the probe, a force map was generated after palpating area A, as shown in Fig. 17 (b), together with the standard deviation of each sensing element shown in Fig. 17 (c). Through the force map, locations of the hard nodules can be easily visualized. The tests demonstrated that the interaction forces measured by the sensing elements exceeded the value 0.4 N when the probe was in contact with a nodule. Force feedback from the left nodule was higher than force feedback from the right one, due mainly to the size of the nodule [15]. On the contrary, in nodule-free area, outputs of each sensing element varied mostly in the range of 0.15–0.25 N, within which the noise level was within an acceptable range compared to the interaction force level.

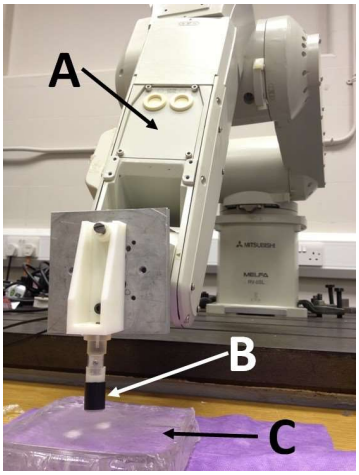

Fig. 16. Integration of fiber optics tactile probe head with robot arm (A: Robot manipulator, B: Tactile probe head, C: Silicone phantom).

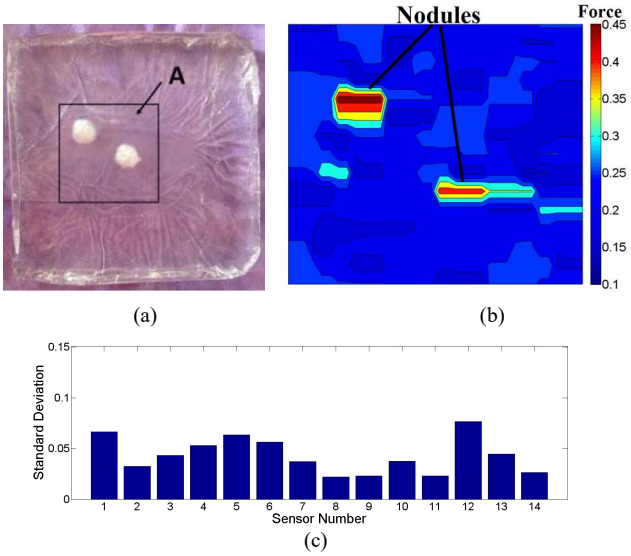

Fig. 17. (a) Palpation test in area A on silicone phantom tissue with two nodules embedded (diameter: left: 10 mm, right: 8 mm), (b) Test results of area A, (c) Standard deviation of each sensing element.

After evaluating the performance on silicone phantom tissue, a lamb kidney with an embedded nodule was tested. The nodule was made of rubber with an elastic modulus of 79.5 kPa tested by Instron 5565 (Instron, Canton, MA) [45]. The diameter of the nodule was 8mm and it was much stiffer than the lamb kidney, with a Young's modulus of 5.9±0.7 kPa [46]. It was buried close to the kidney surface, shown in Fig. 18 (a). As an uneven tissue surface would have affected the effectiveness of the stiffness map [47] generated by the developed tactile probe head, the hard nodule was embedded beneath a relatively flat area B for palpation testing. During tests, the probe palpated the kidney following the same procedure used when palpating the silicone phantom to cover area B. The test results for kidney palpation are shown in Fig. 18 (b) (c). By combining sensor outputs and the palpating positions of the probe head, the force map of area B was created. It can clearly be seen from the force map that the forces concentrated in the central area of B which coincided with the location of the hidden nodule. The uneven force distribution from the rest of this stiffness map and standard deviation of each sensing element during the repeated test may have been caused by the non-flat property of the tissue, together with the noise from shear force and fiber bending. Nevertheless, these values were kept in the range of 0–0.1 N which did not affect the effectiveness of our tactile probe head in tumor localization accuracy. Compared to the silicone phantom tissue, lamb kidney is softer and can be easily damaged requiring a flexible and sensitive palpation device, and the proposed one has shown its capability of conducting accurate and effective tissue palpation for tissue abnormality detection.

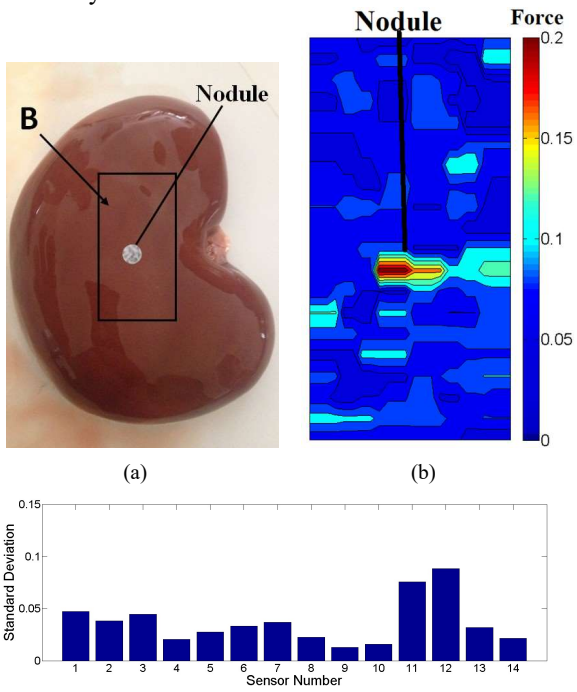

Fig. 18. (a) Lamb kidney sample with invisible nodule buried in area B, (b) Test results of the tactile sensor, (c) Standard deviation of each sensing element.

IV. Discussion and Conclusion

This paper presents a laboratory prototype tactile probe head for detecting abnormal tissue during palpation in open as well as minimally invasive surgery. The probe's tactile sensing accuracy in detecting nodules has been shown in the relevant tests. The probe head can measure the normal force and its spatial distribution over the sensor's surface based on light intensity modulation. The force is detected and calculated by a single camera system using a pixel-based method making the proposed device low cost and ideal for high density tactile array sensing. The sensor is suitable to a medical environment as it uses fiber optics which is lightweight, not susceptible to electromagnetic noise and easily sterilized. The absence of metallic materials and electrical signals from the sensing area make this sensor MRI compatible too.

Future research will focus on 3-axis sensing as the current designed sensor provides only uniaxial force feedback which can be affected by high shear forces. This will enable us to further investigate the relationship between applied force by the surgical instrument and tissue reaction force applied on the sensing nodes. In addition, further miniaturization will be carried out, aiming at allowing the probe head to fit through a trocar

port of 8 mm diameter during MIS. Future work will also focus on instantaneous measurement of indentation depth in order to palpate non-flat surfaces and on extending the sensor spatial resolution by taking advantage of the large number of pixels available on camera images.

References

[1] T. Coles, D. Meglan, and N. John, "The role of haptics in medical training simulators: a survey of the state of the art," *Haptics, IEEE Trans.*, vol. 4, no. 1, pp. 51–66, 2011.

[2] M. Ayyildiz, M. Yildiz, and C. Basdogan, "An Opto-Electro-Mechanical Tactile Sensor for Detection of Breast Lumps," *Haptics, IEEE Trans.*, vol. 6, no. 2, pp. 145–155, 2012.

[3] Q. Peng, S. Omata, D. M. Peehl, and C. E. Constantinou, "Stiffness mapping prostate biopsy samples using a tactile sensor.," *Conf. Proc. IEEE Eng. Med. Biol. Soc.*, vol. 2011, pp. 8515–8, Jan. 2011.

[4] Y. Park and J. W. Ha, "Comparison of one-level posterior lumbar interbody fusion performed with a minimally invasive approach or a traditional open approach.," *Spine (Phila. Pa. 1976).*, vol. 32, no. 5, pp. 537–543, 2007.

[5] J. Rosen, B. Hannaford, M. P. MacFarlane, and M. N. Sinanan, "Force controlled and teleoperated endoscopic grasper for minimally invasive surgery--experimental performance evaluation.," *IEEE Trans. Biomed. Eng.*, vol. 46, no. 10, pp. 1212–21, Oct. 1999.

[6] H. Liu, D. P. Noonan, B. J. Challacombe, P. Dasgupta, L. D. Seneviratne, and K. Althoefer, "Rolling mechanical imaging for tissue abnormality localization during minimally invasive surgery.," *IEEE Trans. Biomed. Eng.*, vol. 57, no. 2, pp. 404–14, Feb. 2010.

[7] G.-P. Haber, M. a White, R. Autorino, P. F. Escobar, M. D. Kroh, S. Chalikonda, R. Khanna, S. Forest, B. Yang, F. Altunrende, R. J. Stein, and J. H. Kaouk, "Novel robotic da Vinci instruments for laparoendoscopic single-site surgery.," *Urology*, vol. 76, no. 6, pp. 1279–82, Dec. 2010.

[8] M. V. Ottermo, O. Stavdahl, and T. a. Johansen, "Palpation instrument for augmented minimally invasive surgery," *2004 IEEE/RSJ Int. Conf. Intell. Robot. Syst. (IEEE Cat. No.04CH37566)*, vol. 4, pp. 3960–3964, 2004.

[9] P. Puangmali, K. Althoefer, L. D. Seneviratne, D. Murphy, and P. Dasgupta, "State-of-the-Art in Force and Tactile Sensing for Minimally Invasive Surgery," *IEEE Sens. J.*, vol. 8, no. 4, pp. 371–381, Apr. 2008.

[10] P. Peng, a. S. Sezen, R. Rajamani, and a. G. Erdman, "Novel MEMS stiffness sensor for force and elasticity measurements," *Sensors Actuators A Phys.*, vol. 158, no. 1, pp. 10–17, Mar. 2010.

[11] K. Tadano and K. Kawashima, "Development of 4-DOFs forceps with force sensing using pneumatic servo system," *Proc. 2006 IEEE Int. Conf. Robot. Autom. 2006. ICRA 2006.*, no. May, pp. 2250–2255, 2006.

[12] G. McCreery and A. Trejos, "Feasibility of locating tumours in lung via kinaesthetic feedback," *Int. J. Med. Robot. Comput. Assist. Surg.*, vol. 4, no. 1, pp. 58–68, 2008.

[13] B. Ahn, Y. Kim, C. K. Oh, and J. Kim, "Robotic palpation and mechanical property characterization for abnormal tissue localization.," *Med. Biol. Eng. Comput.*, vol. 50, no. 9, pp. 961–71, Sep. 2012.

[14] H. Liu, P. Puangmali, D. Zbyszewski, O. Elhage, P. Dasgupta, J. S. Dai, L. Seneviratne, and K. Althoefer, "An indentation depth–force sensing wheeled probe for abnormality identification during minimally invasive surgery," *Proc. Inst. Mech. Eng. Part H J. Eng. Med.*, vol. 224, no. 6, pp. 751–763, Jun. 2010.

[15] H. Liu, J. Li, X. Song, L. D. Seneviratne, and K. Althoefer, "Rolling Identification Probe for Tissue Abnormality During Minimally Invasive Surgery," *IEEE Trans. Robot.*, vol. 27, no. 3, pp. 450–460, 2011.

[16] M. Li, J. Konstantinova, V. Aminzadeh, T. Nanayakkara, L. D. Seneviratne, P. Dasgupta, and K. Althoefer, "Real-time Visual Stiffness Feedback for Soft Tissue Palpation in a Telemanipulation Environment," in *Hamlyn Simposium*, 2013, pp. 77–78.

[17] R. D. Howe, W. J. Peine, D. A. Kantarinis, and J. S. Son, "Remote palpation technology," *Eng. Med. Biol. Mag. IEEE*, vol. 14, no. 3, pp. 318–323, 1995.

[18] E. Petter, M. Biehl, and J. U. Meyer, "Vibrotactite Palpation Instrument for Use in Minimal Invasive Surgery," *Eng. Med. Biol. Soc. 1996. Bridg. Discip. Biomed. Proc. 18th Annu. Int. Conf. IEEE*, vol. 1, pp. 179–180, 1996.

[19] P. Peng and R. Rajamani, "Handheld microtactile sensor for elasticity measurement," *Sensors Journal, IEEE*, vol. 11, no. 9, pp. 1935–1942, 2011.

[20] V. Egorov, S. Ayrapetyan, and A. P. Sarvazyan, "Prostate mechanical imaging: 3-D image composition and feature calculations.," *IEEE Trans. Med. Imaging*, vol. 25, no. 10, pp. 1329–40, Oct. 2006.

[21] A. P. Miller, W. J. Peine, Jae S. Son, and Z. T. Hammoud, "Tactile imaging system for localizing lung nodules during video assisted thoracoscopic surgery," *Robot. Autom. 2007 IEEE Int. Conf.*, pp. 2996–3001, 2007.

[22] a. L. Trejos, J. Jayender, M. T. Perri, M. D. Naish, R. V. Patel, and R. a. Malthaner, "Robot-assisted Tactile Sensing for Minimally Invasive Tumor Localization," *Int. J. Rob. Res.*, vol. 28, no. 9, pp. 1118–1133, May 2009.

[23] A. Talasaz and R. Patel, "Telerobotic palpation for tumor localization with depth estimation," *IEEE/RSJ Int. Conf. Intell. Robot. Syst.*, pp. 463–468, 2013.

[24] B. Kuebler, U. Seibold, and G. Hirzinger, "Development of actuated and sensor integrated forceps for minimally invasive robotic surgery," *Int. J. Med. Robot. Comput. Assist. Surg.*, vol. 01, no. 03, pp. 96–107, 2005.

[25] S. J. Mihailov, "Fiber Bragg grating sensors for harsh environments.," *Sensors (Basel).*, vol. 12, no. 2, pp. 1898–918, Jan. 2012.

[26] R. S. Dahiya, G. Metta, M. Valle, and G. Sandini, "Tactile Sensing—From Humans to Humanoids," *IEEE Trans. Robot.*, vol. 26, no. 1, pp. 1–20, Feb. 2010.

[27] K. Grattan and T. Sun, "Fiber optic sensors: an introduction and overview," in in *Optical Fiber Sensor Technology*, Springer US, 2000, pp. 1–44.

[28] P. Goodyer and J. Fothergill, "The design of an optical fiber pressure transducer for use in the upper airways," *Biomed. Eng. IEEE Trans.*, vol. 43, no. 6, pp. 600–660, 1996.

[29] H. Xie and A. Jiang, "Pixel-based optical fiber tactile force sensor for robot manipulation," in *Sensors conference, 2012 IEEE*, 2012, pp. 1–4.

[30] H. Liu, P. Puangmali, K. a. Althoefer, and L. D. Seneviratne, "Experimental study of soft tissue recovery using optical fiber probe," *2007 IEEE/RSJ Int. Conf. Intell. Robot. Syst.*, pp. 516–521, Oct. 2007.

[31] P. Polygerinos, T. Schaeffter, L. Seneviratne, and K. Althoefer, "A fibre-optic catheter-tip force sensor with MRI compatibility: a feasibility study.," *Conf. Proc. IEEE Eng. Med. Biol. Soc.*, vol. 2009, pp. 1501–054, Jan. 2009.

[32] H. Xie, A. Jiang, H. Wurdemann, H. Liu, L. Seneviratne, and K. Althoefer, "Magnetic Resonance-Compatible Tactile Force Sensor using Fiber Optics and Vision Sensor," *IEEE Sens. J.*, vol. PP, no. 99, pp. 1–1, 2013.

[33] N. J. Ferrier and R. W. Brockett, "Reconstructing the Shape of a Deformable Membrane from Image Data," *Int. J. Rob. Res.*, vol. 19, no. 9, pp. 795–816, Sep. 2000.

[34] H. Yussof, S. C. Abdullah, and M. Ohka, "Development of Optical Three-Axis Tactile Sensor and its Application to Robotic Hand for Dexterous Manipulation Tasks," *2010 Fourth Asia Int. Conf. Math. Model. Comput. Simul.*, pp. 624–629, 2010.

[35] Y. Ito, Y. Kim, and G. Obinata, "Robust Slippage Degree Estimation Based on Reference Update of Vision-Based Tactile Sensor," *IEEE Sens. J.*, vol. 11, no. 9, pp. 2037–2047, Sep. 2011.

[36] Q. Wan, E. Roche, and C. Walsh, "Multifunctional Laparoscopic Trocar With Built-in Fascial Closure and Stabilization Device Design," *J. Med. Device.*, vol. 7, no. September, pp. 3–5, 2013.

[37] H. Xie, H. Liu, and S. Luo, "Fiber optics tactile array probe for tissue palpation during minimally invasive surgery," *IEEE/RSJ Int. Conf. Intell. Robot. Syst.*, pp. 2539–2544, 2013.

[38] P. . Sahoo, S. Soltani, and a. K. . Wong, "A survey of thresholding techniques," *Comput. Vision, Graph. Image Process.*, vol. 41, no. 2, pp. 233–260, Feb. 1988.

[39] S. Al-amri and N. Kalyankar, "Image Segmentation by using threshold Techniques," *arXiv Prepr. arXiv1005.4020*, vol. 2, no. 5, pp. 83–86, 2010.

[40] X. Jiang, I. C. Society, and D. Mojon, "Adaptive Local Thresholding by Verification-Based Multithreshold Probing with Application to Vessel Detection in Retinal Images æ," *Pattern Anal. Mach. Intell. IEEE Trans.*, vol. 25, no. 1, pp. 131–137, 2003.

[41] J.-L. Fan and B. Lei, "A modified valley-emphasis method for automatic thresholding," *Pattern Recognit. Lett.*, vol. 33, no. 6, pp. 703–708, Apr. 2012.

[42] P. Puangmali, L. D. Seneviratne, P. Dasgupta, and K. Althoefer, "Miniature 3-Axis Distal Force Sensor for Minimally Invasive Surgical Palpation," *IEEE/ASME Trans. Mechatronics*, vol. 17, no. 4, pp. 646–656, Aug. 2012.
[43] M. P. Ottensmeyer, "Minimally Invasive Instrument for In Vivo Measurement of Solid Organ Mechanical Impedance," PhD Thesis, Massachusetts Institute of Technology, 2001.
[44] N. McDannold and S. E. Maier, "Magnetic resonance acoustic radiation force imaging," *Med. Phys.*, vol. 35, no. 8, pp. 3748–3758, 2008.
[45] K. Sangpradit, H. Liu, P. Dasgupta, K. Althoefer, and L. D. Seneviratne, "Finite-element modeling of soft tissue rolling indentation.," *IEEE Trans. Biomed. Eng.*, vol. 58, no. 12, pp. 3319–3327, Dec. 2011.
[46] V. Egorov, S. Tsyuryupa, S. Kanilo, M. Kogit, and A. Sarvazyan, "Soft tissue elastometer," *Med. Eng. Phys.*, vol. 30, no. 2, pp. 206–212, 2008.
[47] A. Talasaz and R. Patel, "Integration of Force Reflection with Tactile Sensing for Minimally Invasive Robotics-Assisted Tumor Localization," *Haptics, IEEE Trans.*, vol. 6, no. 2, pp. 217–228, 2013.

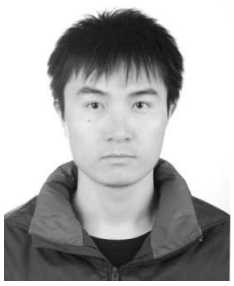

Hui Xie received his B.Eng. degree in Automatic Control from Northwestern Polytechnical University, Xi'an, China, in 2010. He is funded by King's-China Scholarship Council and currently working toward his Ph.D. degree in tactile force sensors in the Center for Robotics Research, Department of Informatics, King's College London, London, U.K. He is a student member of IEEE. His research interests include fiber optics, tactile sensing system and image processing.

Hongbin Liu is currently a lecturer (Assistant Professor) in the department of Informatics, King's College London, UK. He received his B.S. degree in 2005 from the Northwestern Polytechnique University, Xi'an, China, and was awarded with an MSc degree from King's College London in 2006. He received his PhD in 2010 from Kings College London. He is a member of IEEE. His research interests include tactile/force perception based robotic cognition, modeling of dynamic interaction, medical robotics and haptics.

Lakmal D. Seneviratne (M'03) received the B.Sc. (Eng.) and Ph.D. degrees in mechanical engineering from King's College London, London, U.K., in 1980 and 1985, respectively. He is currently a Professor of Robotics at Khalifa University, Abu Dhabi, U.A.E., on secondment from KCL, where he is a Professor of Mechatronics. He has published over 250 refereed research papers related to robotics and mechatronics. His research interests include robotics and intelligent autonomous systems. Prof. Seneviratne is a Fellow of the Institution of Engineering (IET) and Technology and the Institution of Mechanical Engineers (IMechE).

Kaspar Althoefer (M'03) received his Dipl.-Ing. degree in electronic engineering from the University of Aachen, Aachen, Germany, and his Ph.D. degree in electronic engineering from King's College London, London, U.K. He is currently a Professor of Robotics and Intelligent Systems and Head of the Centre for Robotics Research (CoRe), Department of Informatics, King's College London. He has been involved in research on mechatronics since 1992 and gained considerable expertise in the areas of sensing, sensor signal analysis, embedded intelligence, and sensor data interpretation using neural networks and fuzzy logic, as well as robot-based applications He has authored or coauthored more than 180 refereed research papers related to mechatronics and robotics.